Electronic Supplementary Material (ESI) for Journal of Materials Chemistry A.

Supporting Information

for

In-situ Formation of a Multicomponent Inorganic-rich SEI Layer Provides a Fast Charging and High Specific Energy Li-metal Battery

Ho-Hyun Sun,[a] Andrei Dolocan,[b] Jason A. Weeks,[c] Rodrigo Rodriguez,[a] Adam Heller,[a] and C. Buddie Mullins*[a,c]

[a]McKetta Department of Chemical Engineering, The University of Texas at Austin, Texas 78712-1589, United States

[b]Texas Materials Institute, University of Texas at Austin, Austin, Texas 78712-1224, United States

[c]Department of Chemistry, The University of Texas at Austin, Texas 78712-1224, United States

Keywords: Li-metal battery, solid-electrolyte interphase layer, electrolyte solution, fast charging, $Li[Ni_{0.6}Co_{0.2}Mn_{0.2}]O_2$ cathode

Experimental

Sample Preparation

Three solutions of 3:1 v/v EMC (99+%, TCI): FEC (99+%,TCI) (termed EF31) were made with (i) *10EF31P,* comprising 1 M LiTFSI (Sigma-Aldrich 99.95 %), 0.05 M $LiPF_6$ (BASF 99.8%); (ii) *82EF31P*, comprising 0.8 M LiTFSI; 0.2 M LiDFOB (Sigma-Aldrich) and 0.05M $LiPF_6$; and (iii) *64EF31P* comprising 0.6 M of LiTFSI; 0.4 M of LiDFOB and 0.05M $LiPF_6$. The lithium salts were vacuum dried, and the solvents were dried over alumina molecular sieve (Sigma-Aldrich). The Li metal foil (Hohsen Corp.) was used as received; the $Li[Ni_{0.59}Co_{0.2}Mn_{0.2}Al_{0.1}]O_2$ (NCM622-Al 1%) cathode material was a gift of the Sun lab at Hanyang University, Korea.[S1]

Electrochemical Characterization and Testing

Pairs of 5/8'' diameter Li electrodes were tested in 2032 coin-type cells. 100 μL of electrolyte was added to each cell and the cells were cycled galvanostatically at a current density of 0.9, 1.8, and 3.6 mA cm^{-2} with a deposition/stripping time of 1 hour each. The Li^+ transference number (t_+) was obtained with the symmetrical Li/Li cell by applying a DC voltage of 10 mV and measuring the resulting current. Average Coulombic efficiencies were determined in cells made with a Li metal foil electrode and a bare Cu electrode on which 4 mAh cm^{-2} of Li was deposited and stripped at 0.4 mA cm^{-2} until the voltage reached 1 V. Afterwards, 4 mAh cm^{-2} lithium was deposited/stripped at repeatedly for 15 cycles, then 0.5 mAh cm^{-2} was deposited in the terminal deposition half-cycle. The plated Li on Cu was then fully stripped at 0.4 mA cm^{-2} to 1 V.

Cells, termed LMBs, with 5/8'' diameter lithium foil lithium metal anodes and NCM622 cathodes were built with a Celgard 2400 separator and with the 82EF31P electrolytic solution. The NCM622 cathodes were prepared by mixing with Super-P carbon and polyvinylidene fluoride (PVdF) 90:5.5:4.5 ratio and casting onto an Al foil, resulting in a loading of ~ 10 mg cm^{-2}. The LMBs cells were cycled at 1 C rate (180 mA g^{-1}) between 2.7 V and 4.3 V vs. Li/Li^+ at 30 °C. For the rate capability test, the LMB cells were cycled from 0.1 C rate to 5.0 C rate. For the electrochemical impedance spectroscopy (EIS), a Gamry Interface 1010E potentiostat was used and the Cu foil was treated with 1 M HCl solution to eliminate surface impurities. The measurements were at the 1 MHz to 1 Hz frequency range at ±10 mV amplitude after formation cycling then after 50 cycles. The Nyquist plots were created using ZView software

and electrolyte conductivity was determined using the EIS measurement data and the following equations were used:[S4,S5]

$$\delta \text{ (S cm}^{-1}\text{)} = \text{K/R}$$

$$K(cm^{-1}) = (l(Distance, cm))/(s(Surface\ area,\ cm2))$$

$$l = 100\mu m,\ s = 0.502cm2$$

where δ is the electrolyte conductivity (S cm^{-1}), K is a constant, R is the resistance (Ω), l is the distance (cm), and s is the surface area (cm^2).

Analytical Techniques

Scanning electron microscopy (SEM, FEI Quanta 650) images were obtained by depositing Li on a Cu foil using a Li/Cu cell configuration in a 2032 coin-type cell and optical deposition images were obtained using an optical cell previously reported before.[S2,S3] The chemical composition of the SEI surface was measured utilizing a Kratos Axis Ultra X-ray photoelectron spectroscopy (XPS) to interrogate the Li deposited on the Cu substrate. Data was taken using a monochromatic Al-Kα X-ray source (hν = 1486.5 eV) with a spot size of 300 x 700 μm^2. Binding energies were calibrated using the adventitious carbon peak in the C 1s spectra aligned to 284.8 eV. A TOF-SIMS 5 by ION-TOF GmbH, 2010 was used to measure the chemical composition as function of depth (that is, the depth profile) of the SEI and quantify the quantity of dead lithium after 10 cycles of deposition/stripping on the Cu foil. For depth profiling in negative polarity a Cs^+ beam (~ 40 nA at 0.5 keV or ~70 nA at 2 keV) was used to sputter a 300 x 300 μm^2 area and a Bi^+ analysis beam (~4 pA, 30 keV) was raster scanned over a 100 x 100 μm^2 area inside the regressing Cs-sputtered area. The negative polarity detection mode is used to identify most of the SEI composition. To detect the dead lithium, we performed depth profiling in positive polarity. In this mode, we keep all the sputtering conditions unchanged except switching the sputtering beam from Cs^+ to O_2^+ (~500 nA, 2 keV). Non-interlaced mode was used to acquire all depth profiles, that is sputtering, and surface analysis is done sequentially. For high resolution imaging at various depths we set the analysis ion gun in the fast imaging mode with 7 bursts (~200 nm lateral resolution, ~0.04 nA Bi^+ sample current). Note that SEM, XPS, and TOF-SIMS samples were all kept under inert conditions using a vacuum transfer chamber.

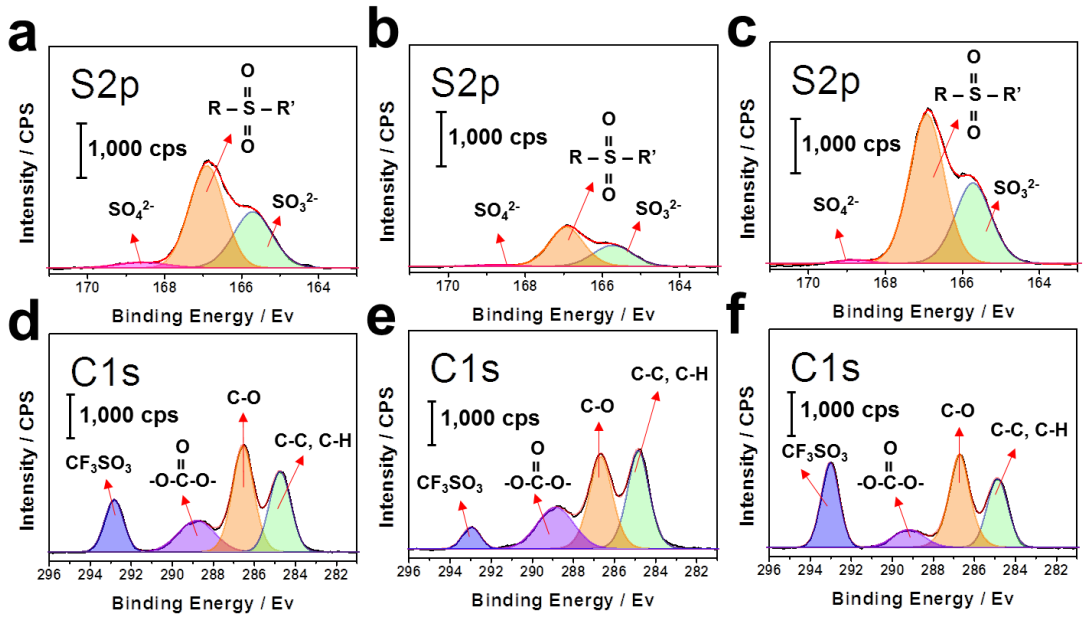

Figure S1. XPS spectra of S2p (a, b, c) and C1s (d, e, f) of the SEI layers after 1st deposition/stripping in Li/Cu cells: (a and d) 10EF31P, (b and e) 64EF31P, and (c and f) 82EF31P.

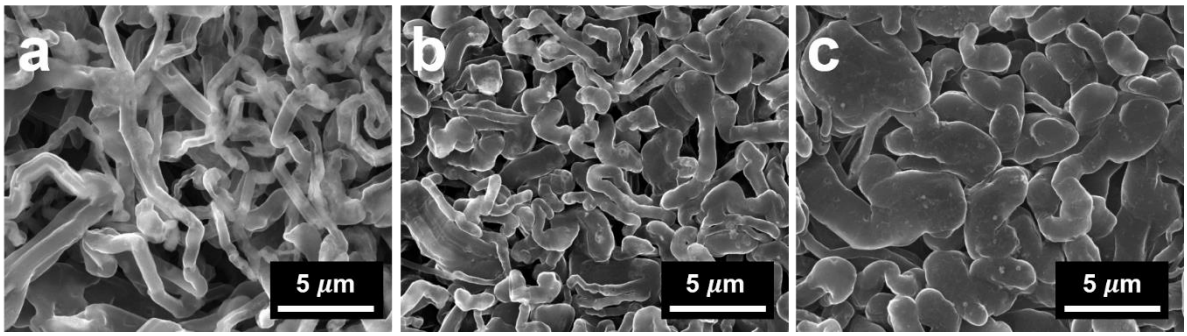

Figure S2. Comparison of SEM images of deposited Li morphologies from Li/Cu cell using different electrolyte solutions at 0.9 mA cm^{-2}: (a) 10EF31P, (b) 64EF31P, and (c) 82EF31P.

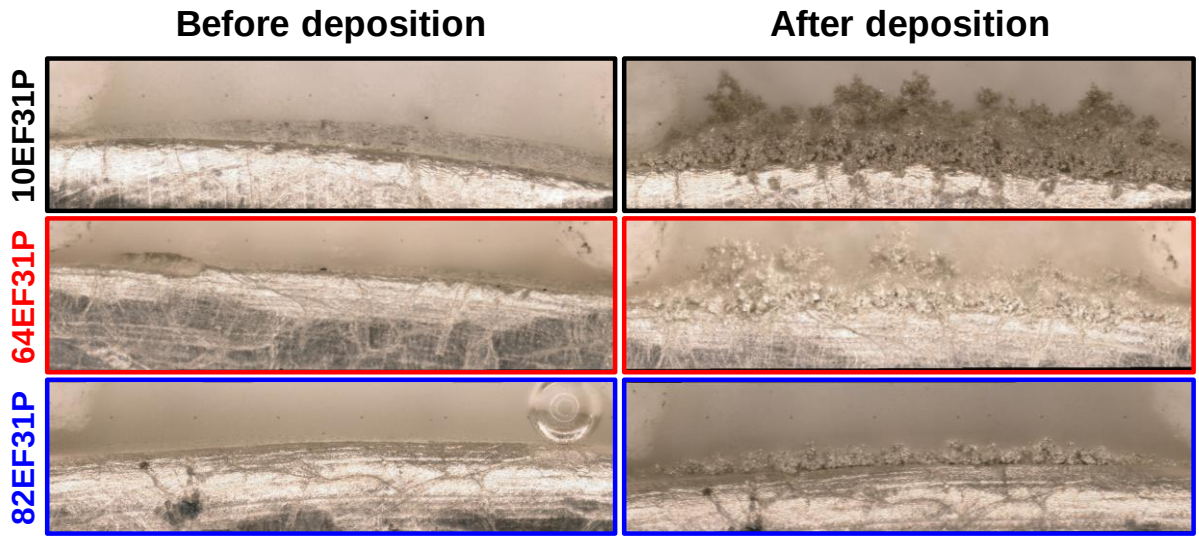

Figure S3. Comparison of optical images of deposited Li morphologies from Li/Li optical cell using 10EF31P (black), 64EF31P (red), and 82EF31P (blue) at 1.8 mA cm^{-2} for 1 hour.

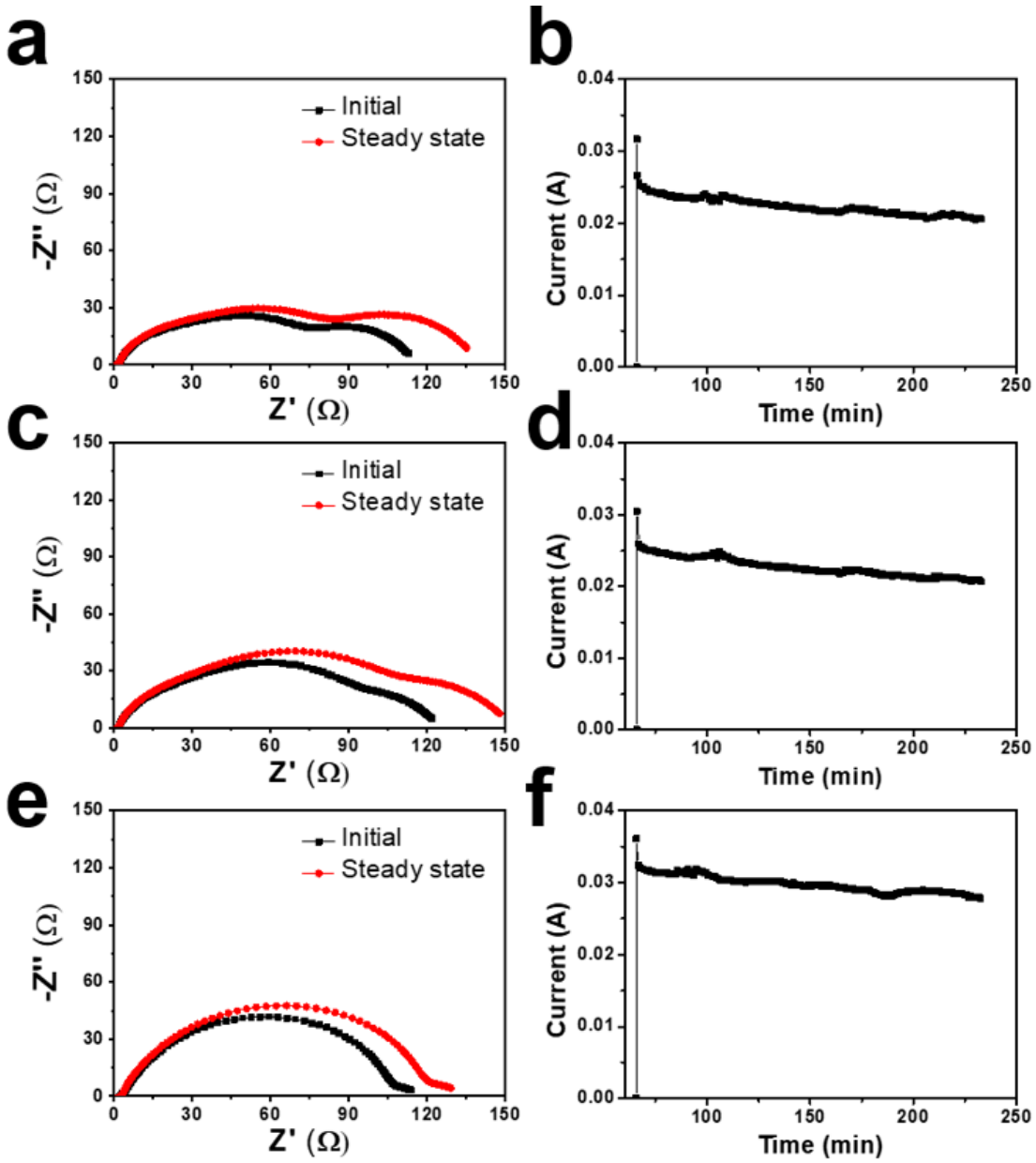

Figure S4. Impedance responses and chronoamperometry profiles of the Li/Li cells with (a and b) 10EF31P, (c and d) 64EF31P and (e and f) 82EF31P electrolytes.

Table S1. Calculated transference number values of 10EF31P, 64EF31P, and 82EF31P electrolyte solutions

Electrolyte	10EF31P	64EF31P	82EF31P
t_{Li+}	0.476	0.493	0.525

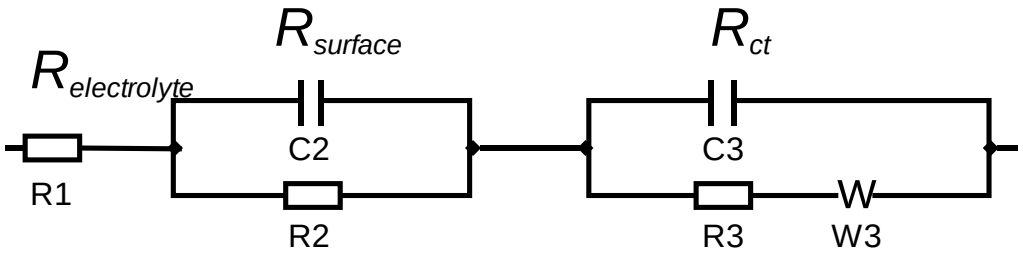

Figure S5. Equivalent circuit model of the EIS Li/Li cells of Figure S4.

Table S2. Comparison of electrolyte conductivity values obtained directly by EIS measurements.

Electrolyte	Resistance (R, Ω)	Conductivity (δ, S cm^{-1})
10EF31P	**8.32**	**2.39×10^{-3}**
64EF31P	**9.74**	**2.04×10^{-3}**
82EF31P	**8.82**	**2.26×10^{-3}**

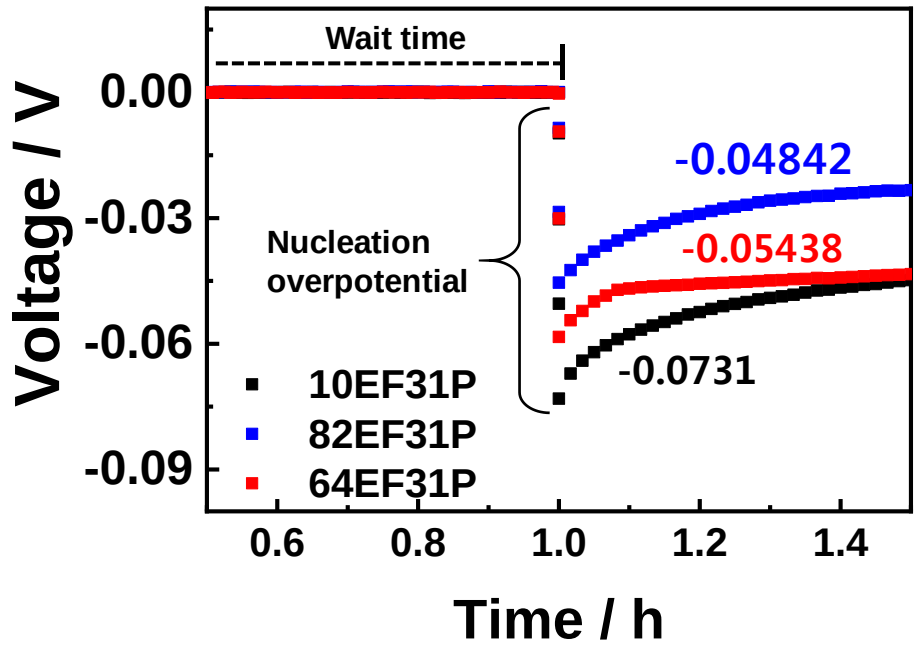

Figure S6. Initial overpotential values measured in Li/Li cells after 1 hour of wait time.

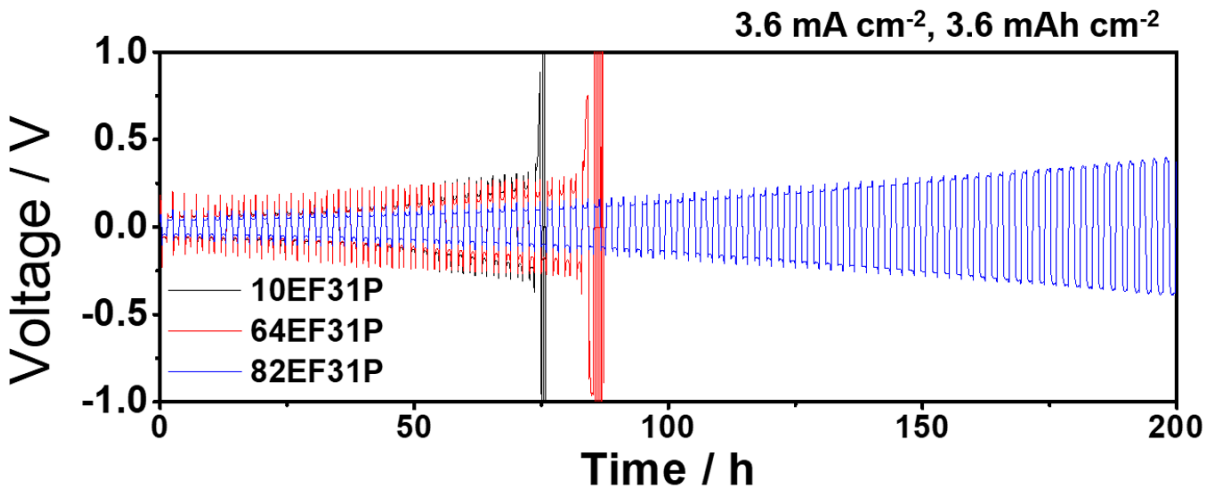

Figure S7. Voltage excursions during the galvanostatic Li deposition/stripping cycles of Li/Li cells at 3.6 mA cm^{-2} with the three different electrolytes.

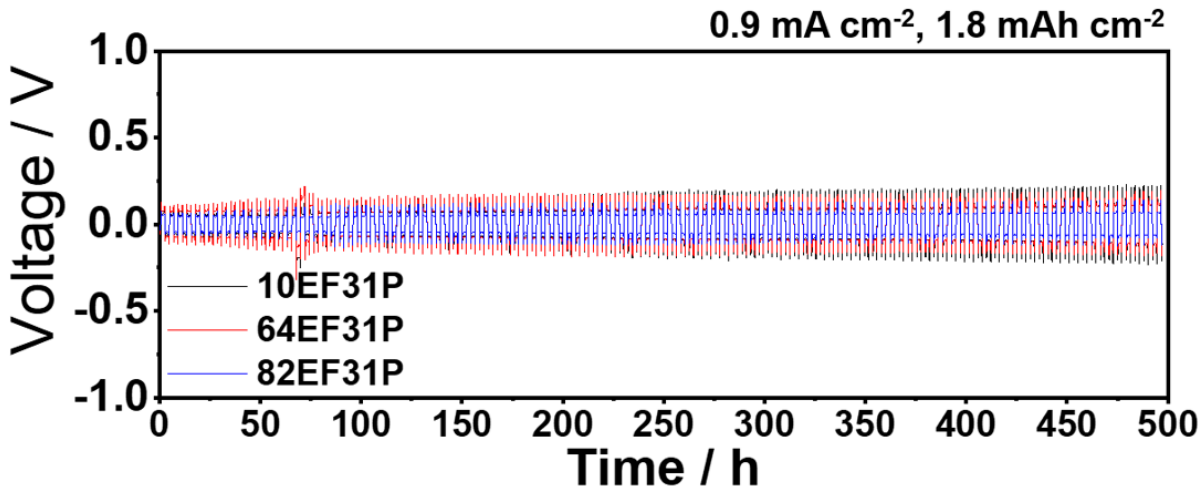

Figure S8. Voltage excursions during the galvanostatic Li deposition/stripping cycles of Li/Li cells at 0.9 mA cm^{-2} with the three different electrolytes.

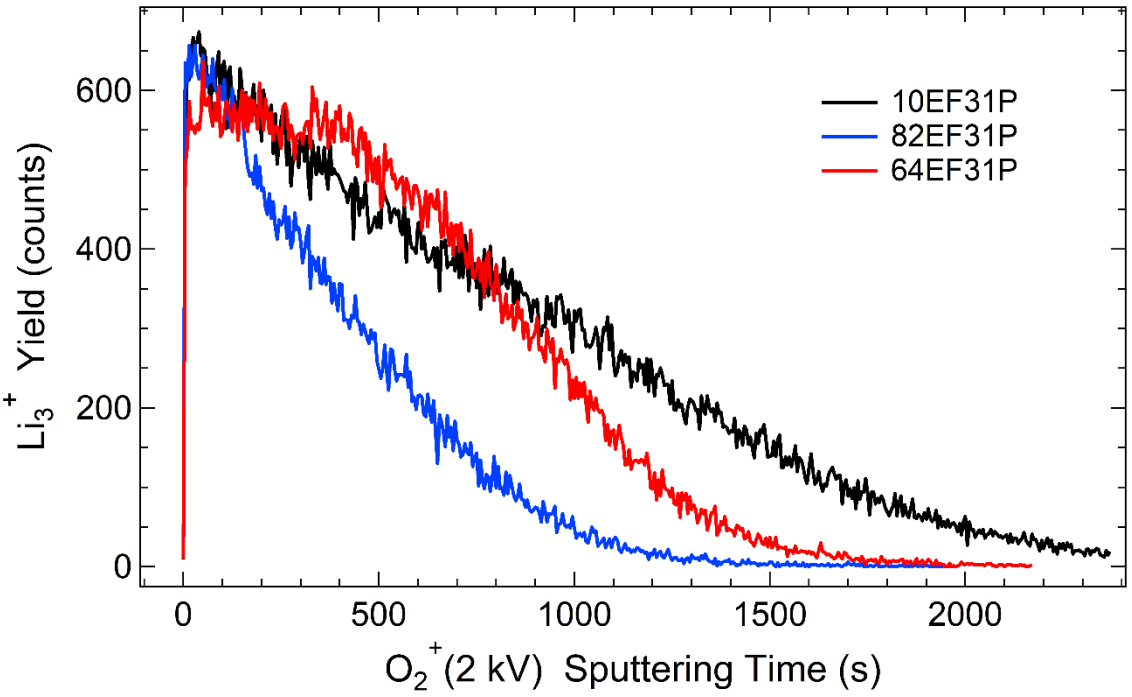

Figure S9. Direct comparison between the dead lithium yield as a function of depth (that is, TOF-SIMS depth profiles) on the three samples showing the largest depth of penetration on the 10EF31P.

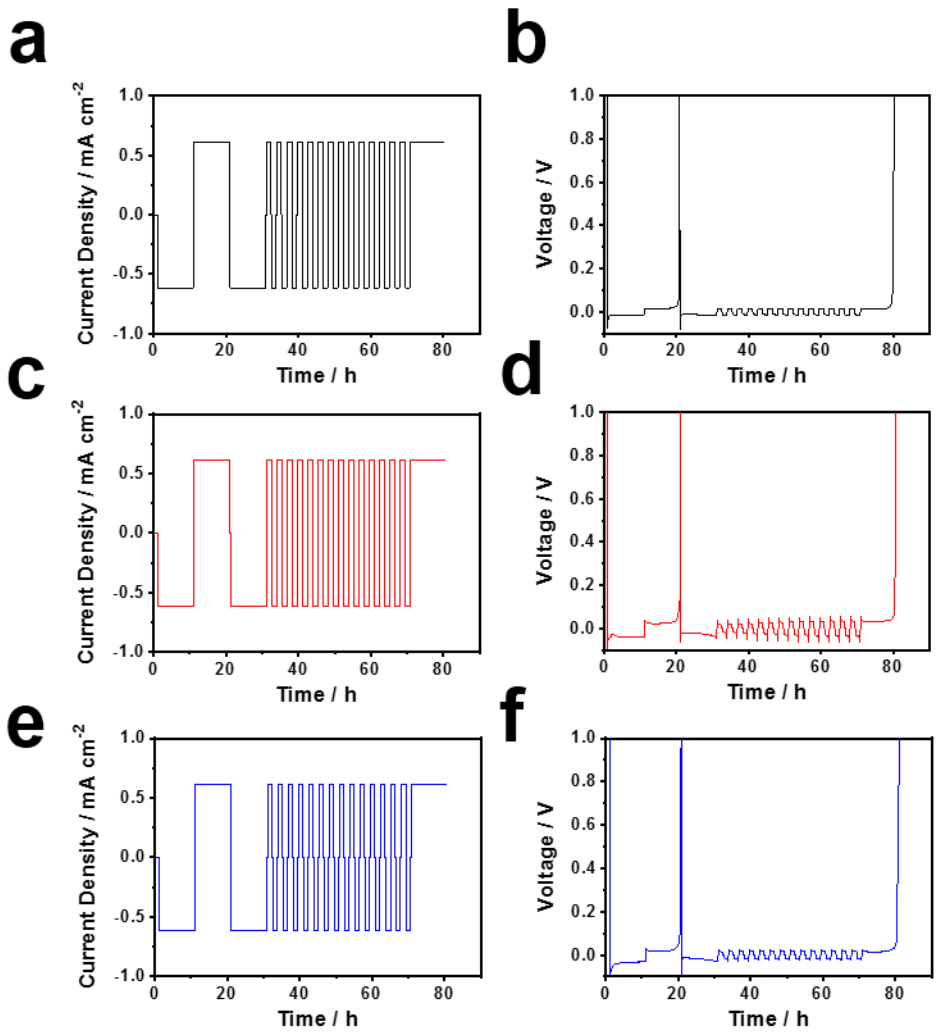

Figure S10. (a, c and e) The constant current protocol and (b, d and f) the measured voltage versus time plot for the Li/Cu cells.; 10EF31D (a and b), 64EF31D (c and d) and 82EF31D (e and f).

Table S3. Average Coulombic Efficiency values of Li/Cu cells of the different electrolyte solutions.

Electrolyte	10EF31D	64EF31D	82EF31D
Average Coulombic Efficiency	97.0%	98.3%	98.8%

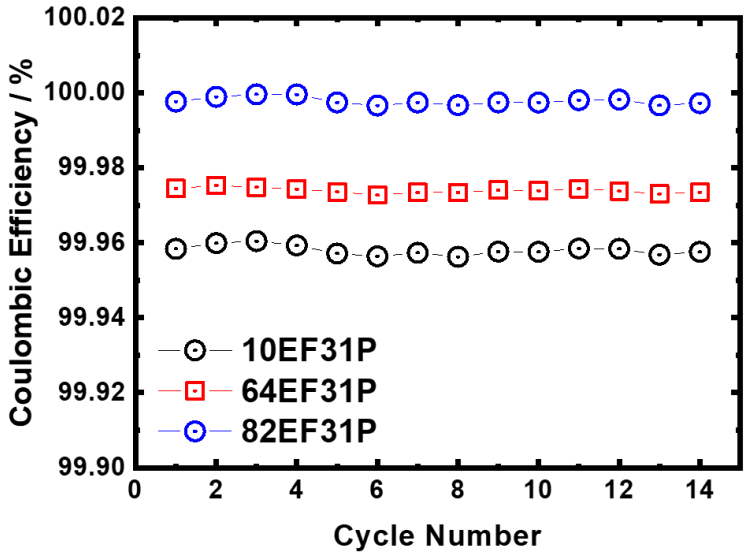

Figure S11. Coulombic efficiency versus cycle number of the Li/Cu cells with different electrolyte.

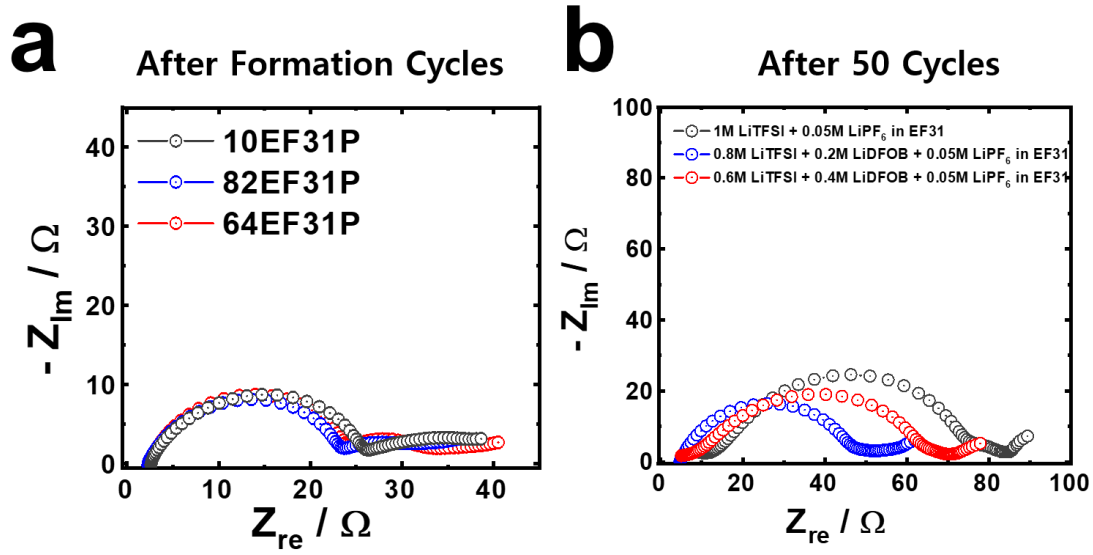

Figure S12. Electrochemical impedance spectroscopy of Li/Cu symmetrical cells with different electrolyte solutions measured (a) after formation cycle and (b) after 50 cycles.

Table S4. EIS values of 10EF31P, 64EF31P, and 82EF31P measured after formation cycle and after 50 cycles.

Sample	10EF31P	64EF31P	82EF31P
After Formation	22.5 Ω	20.6 Ω	20.1 Ω
After 50 Cycles	65.3 Ω	52.8 Ω	37.7 Ω

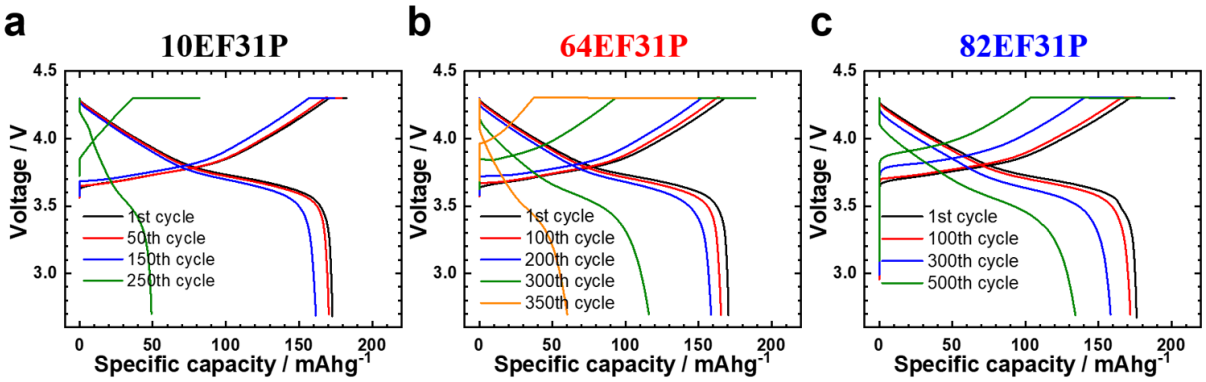

Figure S13. Voltage profile of a Li/NCM622 cell with (a) 10EF31P, (b) 64EF31P, and (c) 82EF31P electrolytes with cathode loading of 10 mg cm^{-2} cycled at a high current density of 1.8 mA cm^{-2}.

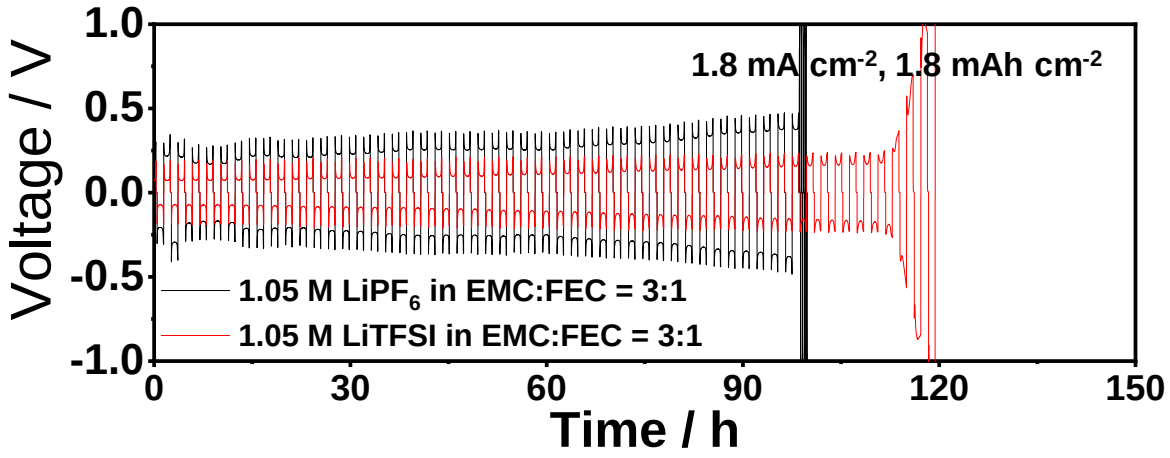

Figure S14. Voltage excursions during the galvanostatic Li deposition/stripping cycles of Li/Li cells at 1.8 mA cm^{-2} with the 1.05 M $LiPF_6$ and 1.05 M LiTFSI in EMC:FEC = 3:1 electrolytes.

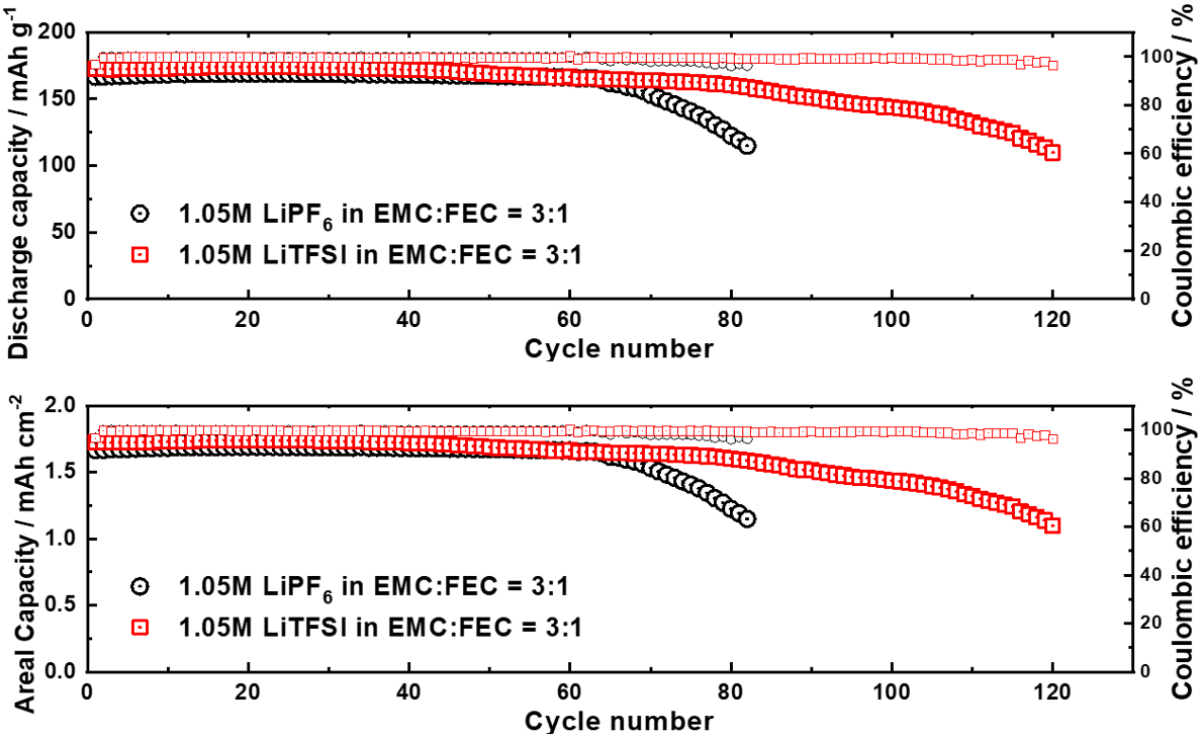

Figure S15. Long-term cycling performance of a Li/NCM622 cell with different electrolytes with cathode loading of 10 mg cm^{-2} cycled at a high current density of 1.8 mA cm^{-2} where the top graph is in discharge capacity (mAh g^{-1}) while the bottom graph is in areal capacity (mAh cm^{-2}).

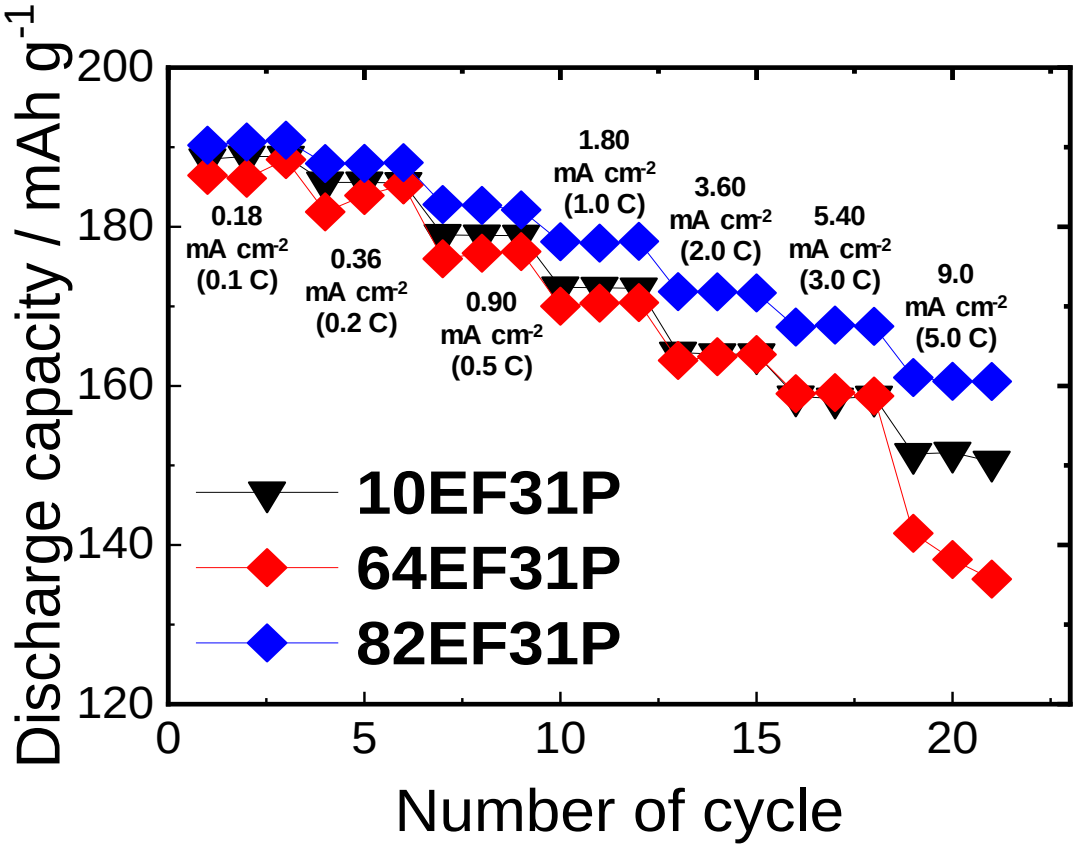

Figure S16. Rate capability test and charge/discharge curves from three different electrolyte cells at the same charge/discharge current.

Table S5. Table comparing the electrochemical performance of 82EF31P to other electrolyte solution electrochemical performance.

Layered Cathode	Cathode Loading (mg cm^{-2})	Areal capacity (mAh cm^{-2})	Current density (mA cm^{-2})	Cycles	Capacity Retention	Ref	
NCM622	~ 18.3	3.3	0.5	90	88 %	S6.	
NCM523	~ 12.0	1.9	1.8	100	65 %	S7.	
NCM622	~ 10.0	1.8	1.8	250	70 %	S8.	
NCM333	~ 10.0	1.5	0.5	250	95 %	S9.	
NCM622	~ 13.0	2.925	N/A	100	86 %	S10.	
NCM622	**~ 10.0**	**1.75**	**1.8**	**500**	**75 %**	**This Work**	

References

1. M. H. Lee, Y. J. Kang, S. T. Myung, Y.-K. Sun, *Electrochim. Acta*, 2017, **8**, 850.

2. S. M. Woods, C. M. Pham, R. Rodriguez, S. S. Nathan, A. Dolocan, H. Celio, J. P. de Souza, K. C. Klavetter, A. Heller, C. B. Mullins, *ACS Energy Lett*. 2016, **1**, 414 – 419.

3. R. Rodriguez, K. E. Loeffler, R. A. Edison, R. M. Stephens, A. Dolocan, A. Heller, C. B. Mullins, *ACS Appl. Energy Mater.*, 2018, **1**, 5830 – 5835.

4. J.-Y. Hwang, H. M. Kim, Y.-K. Sun, *J. Electrochem. Soc.*, 2018, **165**, A5006 – A5013.

5. S.-J. Park, J.-Y. Hwang, C. S. Yoon, H.-G. Jung, Y.-K. Sun, *ACS Appl. Mater. Interfaces*, 2018, **10**, 17985 – 17993.

6. E. Markevich, G. Salitra, F. CHesneau, M. Schmidt, D. Aurbach, *ACS Energy Lett.*, 2017, **2**, 1321 – 1326.

7. X.-Q. Zhang, X.-B. Cheng, X. Chen, C. Yan, Q. Zhang, *Adv. Funct. Mater.*, 2017, **27**, 1605989.

8. S.-J. Park, S.-J. Hwang, C. S. Yoon, H.-G. Jung, Y.-K. Sun, *ACS Appl. Mater. Interfaces*, 2018, **10**, 17985 – 17993.

9. X. Ren, Y. Zhang, M. H. Engelhard, Q. Li, J.-G. Zhang, W. Xu, *ACS Energy Lett*., 2018, **3**, 14 – 19.

10. X. Fan, L. Chen, X. Ji, T. Deng, S. Hou, J. Chen, J. Zheng, F. Wang, J. Jiang, K. Xu, C. Wang, *Chem.* 2018, **4**, 174 – 185.